J Solid State Electrochem (1998) 2: 394–400

ORIGINAL PAPER

Aishui Yu · Naoaki Kumagai · Zhaolin Liu · Jim Y. Lee

Electrochemical lithium intercalation into WO_3 and lithium tungstates $Li_xWO_{3+x/2}$ of various structures

Received: 28 November 1997 / Accepted: 6 March 1998

Abstract Hexagonal and monoclinic tungsten trioxides WO_3 and hexagonal lithium tungstates $Li_xWO_{3+x/2}$ ($x = 0.10$–0.42) from a soft chemistry route were used as the active cathode material in secondary lithium batteries. The hexagonal structures, regardless of their being an oxide or a tungstate, showed higher specific capacities and better cycling behavior in Li^+ intercalation reactions than the monoclinic form. The presence of pre-allocated lithium (as Li_2O) in hexagonal tungstates decreased the capacity for lithium intercalation. Additionally, the plot of open-circuit voltage (OCV) against the depth of intercalation (n) for anhydrous tungstates showed two straight lines with different slopes that can be related to the structural changes in lithium intercalation. The effective diffusion coefficients of lithium insertion into the host structure, $\tilde{D}$, were also found to be dependent on the structure and the composition of these compounds.

Key words Tungsten trioxide · Lithium tungstate · Cathode material · Lithium intercalation · Structural change

Introduction

In recent years, there has been increasing interest in developing tungsten oxides into an active material for secondary lithium batteries and electrochromic displays [1, 2]. The performance of WO_3 in these applications depends on the structure of the prevailing phase, which is determined by the method of preparation [3–6]. The WO_6 octahedral building blocks joining at the corners can result in a large number of crystalline structures, most notably the hexagonal and monoclinic forms (Fig. 1). The thermodynamics and kinetics of lithium intercalation into the WO_3 hosts are controlled to a large extent by the geometry of the oxide architecture.

Tungstic acids or tungsten oxide hydrates are terms used to describe the solid products that are formed in the acidifcation of Li_2WO_4 solutions by strong acids. Different solid phases may be present, depending on the precipitation conditions [7, 8]. Several so-called tungstic acid C phases containing small amounts of cations, $A_xWO_{3+x/2} \cdot yH_2O$ ($A = Na^+, K^+, NH_4^+$, $x = 0.10$–0.28, $y = 0.50$–0.90), were produced by acidifying W(VI) solutions with 0.5–2 M strong acids at 100 °C. Kinetic and structural studies of electrochemical insertion of Li^+ into the anhydrous forms of $A_xWO_{3+x/2}$ ($A = Na^+, K^+, NH_4^+$, $x = 0.10$–0.28) with the hexagonal tungsten bronze (HTB) structure have also been carried out [9–11].

In our previous work [12], the products from the acidification of aqueous Li_2WO_4 solutions with strong acids at 100 °C and the products from a hydrothermal synthesis involving acidified Li_2WO_4 solutions at 125–200 °C were characterized by chemical analysis, X-ray diffractometry, thermogravimetry and X-ray photon-electron spectroscopy. Structural transformations that occurred during heat treatment and the compositional stability of various tungsten oxide phases have also been discussed. This paper will examine the thermodynamics and kinetics of lithium ion insertion into these oxides when they are used as the cathode material in secondary lithium batteries and the changes in their structures as caused by the insertion reaction.

A. Yu (✉) · Z. Liu · J.Y. Lee
National University of Singapore,
10 Kent Ridge Crescent, Singapore 119260
Fax: +65-872-0785; e-mail: as-yu@imre.org.sg

N. Kumagai
Department of Applied Chemistry and Molecular Science,
Faculty of Engineering, Iwate University,
Morioka 020, Japan

Experimental

Preparation

The preparations of WO_3 hydrates and $Li_xWO_{3+x/2}$ by a soft hemistry route have been described previously [12]. The structures

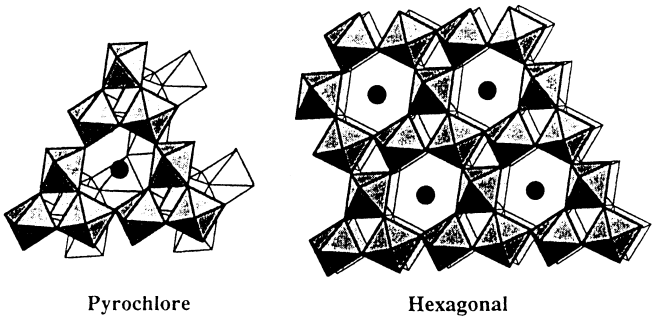

Fig. 1 Structures of hexagonal and monoclinic forms of WO_3

and compositions of the products as determined by atomic absorption spectroscopy and powder X-ray measurements are summarized in Table 1. Atomic absorption spectroscopy was performed on a Hitachi 180-60/80 spectrometer by dissolution of the samples. XRD measurements were carried out using a Rigaku Denki Geiger flux 20B with Cu Kα radiation.

Electrochemical characterizations

The test battery was a three-electrode glass cell filled with Ar. The preparation of the electrodes and electrolyte, the cell design, and the detailed test procedures have been documented elsewhere [13]. The oxides were mixed with graphite in the weight ratio 1:1 and compression-molded onto Ni nets under ca. 50 MPa pressure to achieve a typical loading of ca. 20 mg cm^{-2} of active material. The pellets thus obtained were used as the positive electrodes after drying in vacuum at 80 °C for 1 day. Lithium pellets were used for both the negative and the reference electrodes. The electrolyte was 1 M $LiClO_4$ in propylene carbonate (PC) containing less than 10 mg dm^{-3} of water.

The electrodes were charged and discharged galvanostatically on a Hokuto Denko model HJ-201B charge-discharge unit. Quasi-equilibrium open-circuit voltages (OCVs) were measured after 24 h on open circuit, when the variations in cell voltages were less than 0.2 mVh^{-1}. The cells were also characterized by a.c. impedance measurements in the frequency range 63 kHz–1 mHz. The measurement details can be found in a previous publication [13].

Results and discussion

Charge-discharge profiles

Typical first discharge-recharge curves of hexagonal $WO_3 \cdot 0.60\ H_2O$ and its heat treated (and hence dehydrated) products, measured at a constant current density of 0.2 mA/cm^2 at 25 °C, are shown in Fig. 2. The corresponding cycling behavior of these oxides is given in Fig. 3. The as-synthesized tungsten oxide with a small amount of water, $WO_3 \cdot 0.60\ H_2O$, is higher in initial capacity (220 mAh/g) than anhydrous hexagonal WO_3 (135 mAh/g) that was formed after heating the oxide at 300 °C for 3 h. Anhydrous hexagonal WO_3 also shows better cycling behavior than that of $WO_3 \cdot 0.60\ H_2O$ and monoclinic WO_3 (sample 3 in Table 1) formed upon prolonged heating of $WO_3 \cdot 1.06\ H_2O$. It still delivers nearly 80 mAh/g of charge in the 20th cycle (Fig. 3b), whereas $WO_3 \cdot 0.60\ H_2O$ and monoclinic WO_3 would have their capacities reduced to about 20–50 mAh/g in the same period of time (Fig. 3a and c). Hexagonal forms of WO_3 having large hexagonal tunnels in their structure also display slightly higher discharge potentials than the monoclinic form of the oxide.

In order to establish the influence of the preparation method on the electrochemical behavior of the ensuing oxide products, various tungsten oxides were prepared from 1 M Li_2WO_4 by acidification and by hydrothermal treatment in an autoclave (samples 3–7 in Table 1). The latter method would retain some lithium as Li_2O in the hexagonal tunnels, leading to partial tungstates of the general formula $Li_xWO_{3+x/2}$ ($x = 0$–0.42). The initial charge-discharge curves of these compounds acting as lithium intercalation hosts are shown in Fig. 4, and the changes in their discharge capacity as a function of cycle number are shown in Fig. 5. All hexagonal forms of WO_3 (a,c,d in Figs. 4 and 5) have almost the same electrochemical profile even though they were prepared differently. The recharge efficiency is more than 80% in

Table 1 Compositions and structures of products from different preparation conditions after drying at 100 °C

Sample number	Reaction condition			Composition	Product phase
	Li_2WO_4	HCl	Temp		
1	0.25 M 100 ml	1 M 100 ml	100°C	$WO_3 \cdot 0.60H_2O$	Hexagonal
				WO_3[a]	Hexagonal
2		2 M 100 ml	100°C	$WO_3 \cdot 1.06H_2O(H_2WO_4)$	Layered
				WO_3 [a]	Monoclinic
3	1 M 20 ml	pH = 1.5	100°C	$WO_3 \cdot 0.52H_2O$	Hexagonal
				WO_3[a]	Hexagonal
4			125°C	$Li_{0.10}WO_{3+0.05} \cdot 0.56H_2O$	Hexagonal
				$Li_{0.10}WO_{3+0.05}$[a]	Hexagonal
5			150°C	$Li_{0.20}WO_{3+0.10} \cdot 0.51H_2O$	Hexagonal
				$Li_{0.20}WO_{3+0.10}$[a]	Hexagonal
6			175°C	$Li_{0.36}WO_{3+0.18} \cdot 0.61H_2O$	Hexagonal
				$Li_{0.36}WO_{3+0.18}$[a]	Hexagonal
7			200°C	$Li_{0.42}WO_{3+0.21} \cdot 0.88H_2O$	Hexagonal
				$Li_{0.42}WO_{3+0.21}$[a]	Hexagonal

[a] Anhydrous form (heat treatment in air at 300 °C for 3 h)

the first cycle. It can be concluded from these figures that hexagonal forms of WO_3 with large hexagonal tunnels in their structures have noticeably higher discharge potentials and larger extents of Li^+ insertion (the n values in Li_nWO_3 and $Li_n[Li_xWO_{3+x/2}]$) than hydrothermally formed oxides with pre-allocated Li_2O in the hexagonal tunnels. The discharge potential and discharge capacity would reduce according to the amount of Li_2O in the hexagonal channels. The occupation of available sites for Li^+ intercalation by pre-allocated Li_2O is a likely cause. Other than this, all hexagonal tungstates $Li_xWO_{3+x/2}$ deliver good charge-discharge performance at a constant current density of 0.2 mA/cm^2.

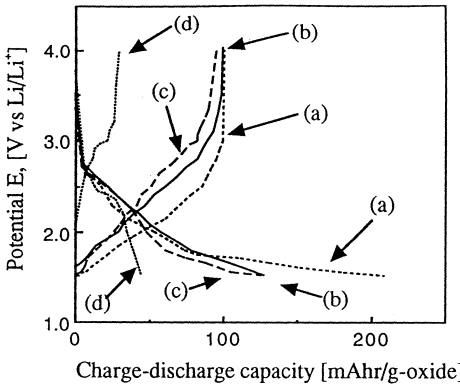

Fig. 2 Initial discharge and recharge curves of $WO_3 \cdot 0.60\ H_2O$ (sample 1 in Table 1) and its heat treated products at a constant current density of 0.2 mA/cm^2: *a* not heat treated, *b* heat treated at 300 °C, *c* heat treated at 350 °C, and *d* heat treated at 400 °C

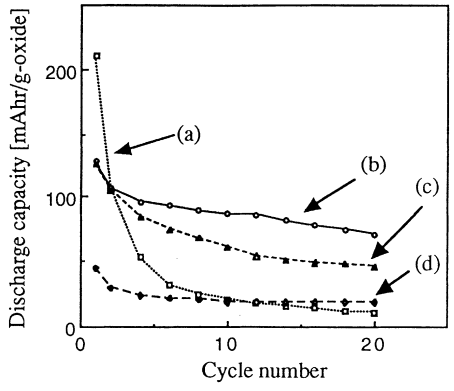

Fig. 3 The discharge capacity of $WO_3 \cdot 0.60\ H_2O$ (sample 1 in Table 1) and its heated products as a function of cycle number: *a* not heat treated, *b* heat treated at 300 °C, *c* heat treated at 350 °C, and *d* heat treated at 400 °C. The electrodes were charged and discharged at a constant current density of 0.2 mA/cm^2 at 25 °C

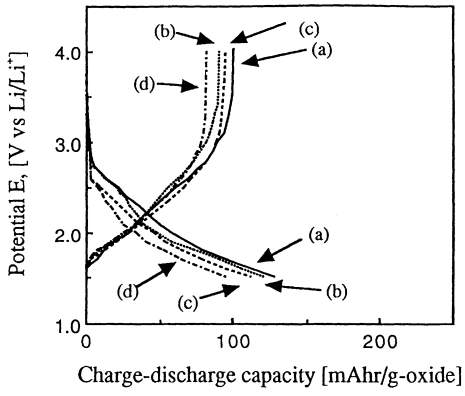

Fig. 4 Discharge-charge curves of several anhydrous $Li_xWO_{3+x/2}$ (x = 0–0.42) electrodes at 0.2 mA/cm^2: *a* WO_3 (sample 1 in Table 1), *b* WO_3 (sample 4 in Table 1), *c* $Li_{0.20}\ WO_{3+0.10}$ (sample 5 in Table 1), and *d* $Li_{0.42}WO_{3+0.21}$ (sample 8 in Table 1)

OCV-*n* curves

The quasi-steady state OCVs are shown in Fig. 6 as a function of the n value in hexagonal Li_nWO_3 and

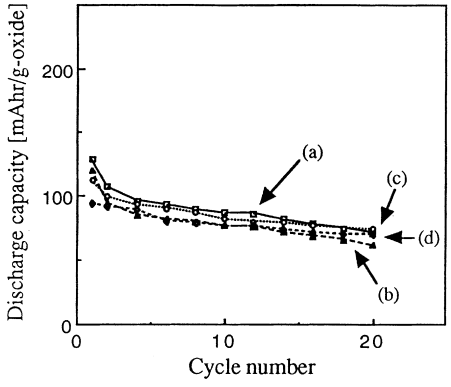

Fig. 5 The discharge capacity as a function of cycle number for several anhydrous $Li_xWO_{3+x/2}$ (x = 0–0.42) electrodes: *a* WO_3 (sample 1 in Table 1), *b* WO_3 (sample 4 in Table 1), *c* $Li_{0.20}\ WO_{3+0.10}$ (sample 5 in Table 1), and *d* $Li_{0.42}WO_{3+0.21}$ (sample 8 in Table 1). The electrodes were charged and discharged at a constant current density of 0.2 mA/cm^2 at 25 °C

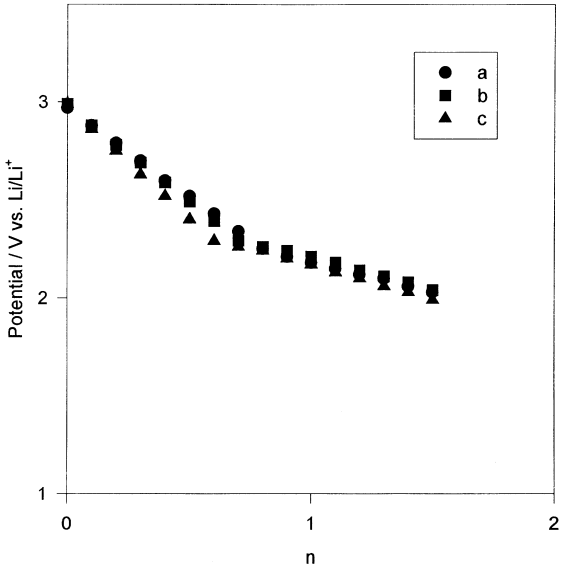

Fig. 6 Open-circuit potential as a function of the depth of intercalation, n, at 25 °C: *a* hexagonal WO_3, *b* hexagonal $Li_{0.20}WO_{3+0.10}$, and *c* hexagonal $Li_{0.42}\ WO_{3+0.21}$

Table 2 The relationships between OCV and n value in $Li_n[Li_xWO_{3+x/2}$ (x = 0–0.42)] and their standard free energies

Compound	Relationship between OCV and n value	ΔG_I^0 (n = 0–1) (kJ/mol)
WO_3	$E = 2.97 - 0.91n (n < 0.8)$, $E = 2.47 - 0.30n (n > 0.7)$	−239.4
$Li_{0.20}WO_{3+0.10}$	$E = 2.98 - 0.97n (n < 0.7)$, $E = 2.12 - 0.30n (n > 0.7)$	−225.4
$Li_{0.42}WO_{3+0.21}$	$E = 2.99 - 1.11n (n < 0.6)$, $E = 2.47 - 0.33n (n > 0.6)$	−219.3

$Li_n[Li_xWO_{3+x/2}$ (x = 0–0.42)]. It can be seen that OCVs decrease linearly with increasing n values in a piece-wise manner, resulting in two straight lines of different slopes. The linearity between OCVs (E) and the n values of several oxide hosts are listed in Table 2. These results suggest that intercalating lithium ions may occupy more than one kind of crystallographic site and that single-phase $Li_n[Li_xWO_{3+x/2}]$ (x = 0–0.42) with continuously varying n is formed. These phenomena were related to the typical voltammetric curves obtained at a low sweep rate of 0.3 mV/s of a hexagonal phase prepared by a soft chemistry; in this case, the cathodic response can be clearly resolved into two peaks at ~ 2.3 and 1.4 V vs Li/Li^+ respectively [9]. The OCV-n relationships are quite different from that of monoclinic WO_3 [12], where "S"-shaped curves were obtained that could be attributed to differences in crystal structures and hence the geometry of the intercalation sites. The OCV values were also higher than that of hexagonal tungstates. The standard free energy of lithium intercalation, ΔG_I^0, in $Li_n[Li_xWO_{3+x/2}]$ (x = 0–0.42) can be calculated from the following equations:

$$\mu m_{Li} - \mu m_{Li}^0 = RT \ln a_{Li} = -FE(n) \quad (1)$$

$$\Delta G = -F \int_0^n E(n)\, dn \quad (2)$$

where n is the depth of lithium intercalation, $E(n)$ is the open circuit potential at the respective n value and μ_{Li}, μ_{Li}^0 and a_{Li} are the lithium chemical potential, the chemical potential for pure lithium and the activity of lithium, respectively [15].

The calculated ΔG_I^0 values for $0 < n < 1$ in $Li_n[Li_xWO_{3+x/2}]$ (x = 0–0.42) are given in Table 2. The free energy of intercalation is found to decrease with the increase in Li_2O content in the structure. As the free energy is an indication of the site energy as experienced by the intercalating lithium ions, the presence of Li_2O in the cavities of hexagonal WO_3 will reduce the site energy and weaken the bond strength between lithium and the host as a result.

Structural variation with lithium intercalation

The variations in the crystal structures of hexagonal WO_3 and hexagonal tungstates $[Li_xWO_{3+x/2}]$ (x = 0–0.42) with the depth of lithium intercalation (n) were examined by XRD. The patterns in Figs. 7 and 8 show that original lattice structures were not altered for lithium intercalation up to $n = 2.0$. The discharged products could be indexed in an orthorhombic cell, and the crystallographic parameters of the discharged products for the oxide with different depths of lithium intercalation are given in Tables 3 and 4. Lithium intercalation is seen to increase the a and b lattice parameters slightly. On the other hand, both the c lattice parameter and the unit cell volume decrease with lithium intercalation at first ($0 < n < 0.5$) but increase with lithium intercalation when n is in the range 0.5–1.5. This dichotomy is similar to the two straight lines of different slopes in the OCV-n plots of Fig. 6. In addition, the b/a ratios for the discharged products are close to $\sqrt{3}$. From the X-ray results one may infer that unsolvated Li^+ ions are located in the empty channels without any perturbation to the hexagonal environment.

Kinetic characteristics of lithium intercalation

The a.c. impedance spectra of hexagonal $Li_{0.5}WO_3$ electrode at 25 °C are shown in Fig. 9. They consist

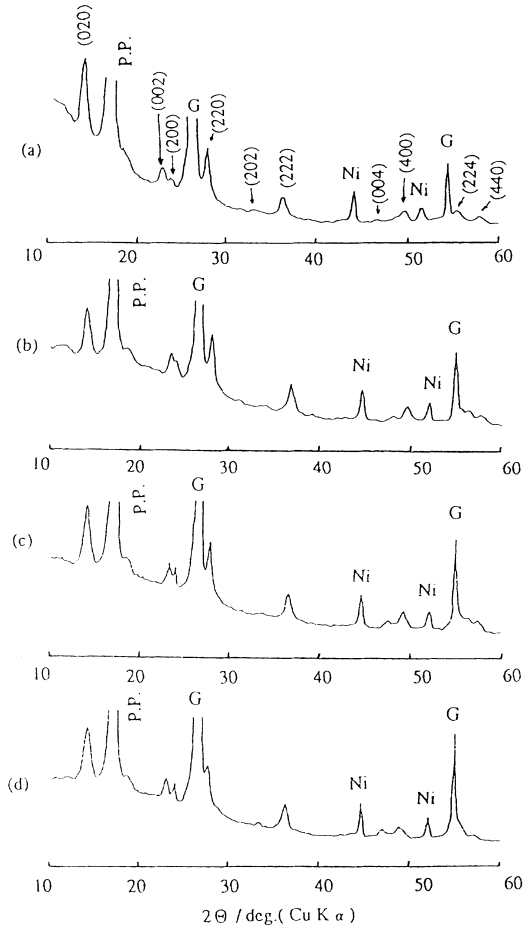

Fig. 7 X-ray diffraction patterns of Li_nWO_3 with various n values: G, graphite; Ni, nickel net; P.P., polypropylene film. *a*, $n = 0$; *b*, $n = 0.5$; *c*, $n = 1.0$; *d*, $n = 2.0$

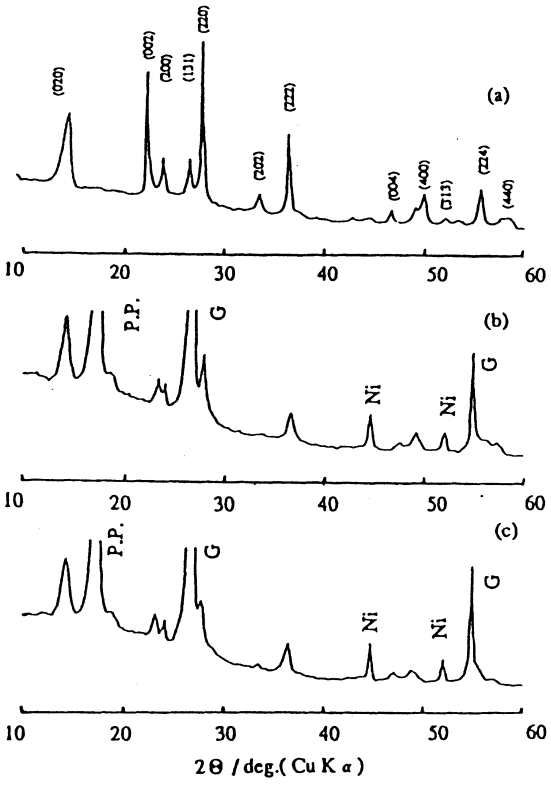

Fig. 8 X-ray diffraction of patterns of $Li_n[Li_{0.42}WO_{3+0.21}]$ with various n values: G, graphite; Ni, nickel net; P.P., polypropylene film. *a*, $n = 0$; *b*, $n = 0.5$; *c*, $n = 1.5$

Table 3 Crystallographic parameters of Li_nWO_3 with different n values

n	Lattice parameter (nm)				Unit cell volume (nm^3)
	a	b	c	a/b	
0	0.7293	1.263	0.7750	1.732	0.7167
0.5	0.7369	1.272	0.7572	1.728	0.7089
1.0	0.7406	1.269	0.7619	1.712	0.7160
2.0	0.7456	1.283	0.7707	1.721	0.7372

Table 4 Crystallographic parameters of $Li_n[Li_{0.42}WO_{3+0.21}]$ with different n values

n	Lattice parameter (nm)				Unit cell volume (nm^3)
	a	b	c	a/b	
0	0.7275	1.262	0.7744	1.734	0.7110
0.5	0.7280	1.265	0.7702	1.737	0.7092
1.0	0.7306	1.270	0.7729	1.738	0.7171
1.5	0.7310	1.275	0.7745	1.744	0.7218

primarily of an irregular semicircular arc in the high-frequency region and an inclined straight line in the low-frequency region. The centre of the circular arc is below the horizontal axis, indicating some microscopic surface roughness in the electrode of the type discussed by de Levie [16]. At low frequencies, the double-layer capacitance becomes completely blocked, and the constant-phase-angle Warburg impedance, Z_w, is clearly resolved. As the low-frequency response can be fitted to a 45 ° straight line, the impedance response can be modelled by the simple Randle's equivalent circuit [17] (Fig. 10), where R_0 is the uncompensated ohmic resistance of the electrode and electrolyte, C_{DL} is the double-layer capacitance of electrode-electrolyte interface, and R_{ct} is the charge transfer resistance. Ho et al. [18] obtained the following expression for Z_w by solving the Fick's law of diffusion with appropriate initial and boundary conditions:

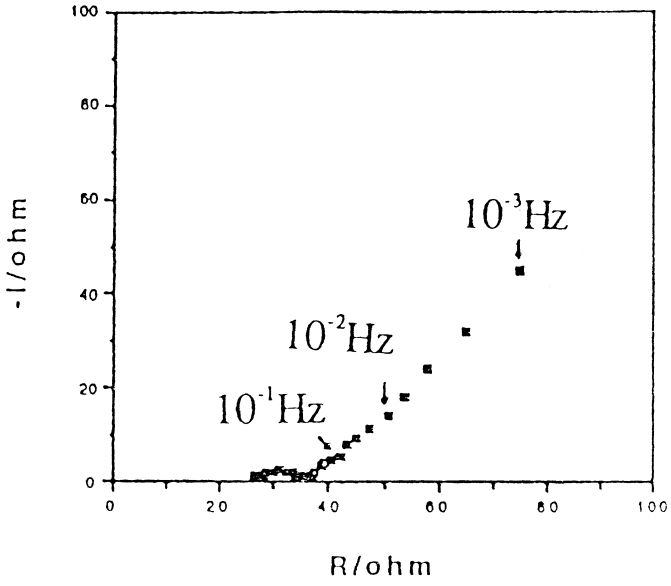

Fig. 9 Impedance spectrum of hexagonal $Li_{0.5}WO_3$ electrode in 1 M $LiClO_4$-PC solution

$$Z_w = A_w \omega^{-1/2} \tag{3}$$

Where ω is the angular frequency of the a.c. perturbation. The Warburg prefactor, A_w, is related to the effective diffusion coefficient, D, of the electroactive species in the electrode by

$$A_w = V_m(dE/dn/zFa\tilde{D}^{1/2} \tag{4}$$

Where V_m is the molar volume of the diffusion medium ($= 37.9$ cm^3 for WO_3) [14], dE/dn is the slope of the OCV-n curve (Fig. 6), z is the charge transfer number for the lithium intercalation reaction, which is equal to 1. The constant a is the effective surface area of the electrode, which is taken to be equal to the geometrical area (1.4 cm^2) in the present study.

Equation 4 shows that the diffusion coefficient depends strongly on the effective surface area. For the porous oxide-graphite composite electrodes used in this study, substitution of the effective surface area by the geometrical area may introduce substantial errors in the values of the diffusion coefficient. On the other hand, the discharge reaction is unlikely to bring about large modifications in the effective surface area; calculation of $\tilde{D}$ based on the geometrical area will still provide useful

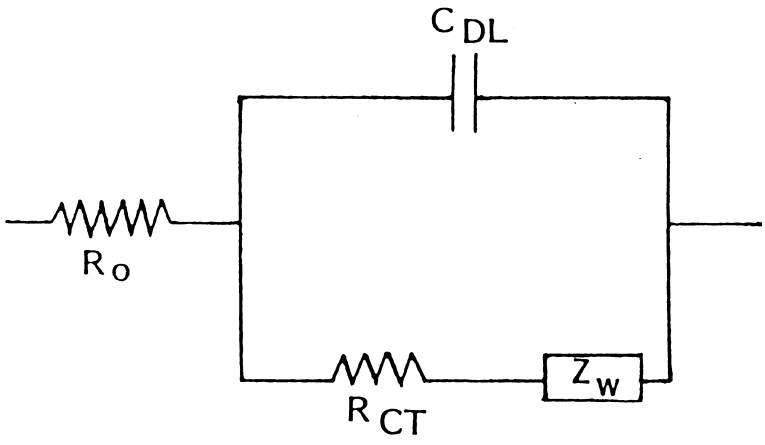

Fig. 10 The Randles equivalent circuit for a.c. impedance response

information on the relative changes in $\tilde{D}$ with the values of n in $Li_n[Li_xWO_{3+x/2}]$ and with the temperature. On this basis several $\tilde{D}$ values were calculated as a function of the depth of lithium intercalation and plotted against the latter in Fig. 11. The $\tilde{D}$ values for Li diffusion in hexagonal structures are about 10^{-9} cm^2/s and two orders of magnitude lower (10^{-11} cm^2/s) in monoclinic WO_3. Li^+ ions also appear to diffuse faster in pure oxides than in hexagonal tungstates $Li_xWO_{3+x/2}$. The deterministic importance of the host structure on lithium intercalation is aptly demonstrated by these observations.

As can be seen from Fig. 1, hexagonal tungsten oxides and tungstates contain large hexagonal tunnels surrounded by six WO_6 octahedra through which two lithium atoms may be incorporated per unit cell. Such wide open architecture enables a faster kinetic response than monoclinic WO_3, in which small tunnels are surrounded by four WO_6 octahedra. In Joo's [19] measurement of the $\tilde{D}$ values in hexagonal $Li_n[0.165K_2O \cdot WO_3]$ thin films by the galvanostatic transient method, the room temperature values were highly anisotropic,varying from the order of 10^{-9}–10^{-10} cm^2/s in the c axis direction to about 10^{-7} cm^2/s in the a axis direction. As the $\tilde{D}$ values in WO_3 and hexagonal tungstates measured here are closer to the values pertaining to diffusion along the c axis, lithium intercalation into polycrystalline $Li_n[Li_xWO_{3+x/2}]$ ($x = 0$–0.42) therefore takes place mainly in the empty hexagonal tunnels of the host structure.

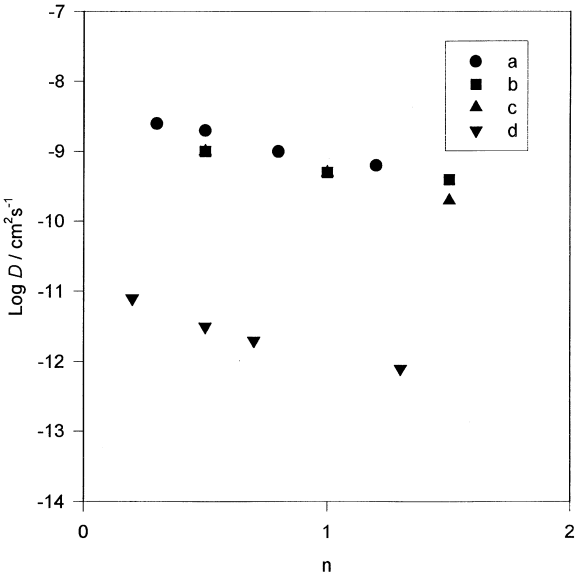

Fig. 11 The effective diffusion coefficient of lithium intercalation, D, as a function of depth of intercalation, n: a hexagonal WO_3, b hexagonal $Li_{0.20}WO_{3+0.10}$, c hexagonal $Li_{0.42}WO_{3+0.21}$, and d monoclinic WO_3

Conclusion

Hexagonal WO_3 and hexagonal tungstates behave similarly in the electrochemical intercalation of Li^+. The behavior is drametrically different from that of the same insertion reaction taking place in a monoclinic structure. The OCV-n curves of hexagonal tungstates consist of two lines with different slopes, reflecting the structural changes that occur during lithium intercalation. The $\tilde{D}$ values for Li^+ diffusion in hexagonal WO_3 and tungstates are 1–2 orders of mangnitude higher than the corresponding values for monoclinic WO_3. It is therefore concluded that the effective diffusion coefficients of lithium intercalation into WO_3 hosts are largely determined by the host architecture.

Acknowledgements The authors would like to thank Mrs. Nobuku Kumagai, Mr. Nanjo Hirowa and Ms. Jie Wei for their experimental assistance.

References

1. Whittingham MS (1988) In: Chowdari BVR, Radhakrishna S (eds) Solid state ionics. World Scientific, Singapore, pp 325–340
2. Reis KP, Ramanan A, Whittingham MS (1992) J Solid State Chem 96: 31
3. Kumagai N, Abe M, Kumagai N, Pereira-Ramos JP, Tanno K (1994) Solid State Ionics 70/71: 451

4. Pereira-Ramos JP, Baddour-Haddour R, Kumagai N, Tanno K (1993) Electrochim Acta 38: 431
5. Guo JD, Whitingham MS (1993) Int Modern Phys B 7: 4145
6. Zhong Q, Dahn JR, Colbow K (1992) J Electrochem Soc 139: 2406
7. Freedman ML (1959) J Am Chem Soc 81: 3834
8. Gerand B, Nowogrocki G, Figlarz M (1981) J Solid State Chem 38: 312
9. Kumagai N, Kumagai N, Umetzu Y, Tanno K, Pereira-Ramos JP (1996) Solid State Ionics 86/88: 1443
10. Kumagai N, Matsuura Y, Kumagai N, Tanno K (1992) J Electrochem Soc 139: 3553
11. Gerand G, Nowagrocki G, Guenot J, Figlarz M (1979) J Solid State Chem 29: 429
12. Kumagai N, Kumagai N, Yu A (1996) Battery Technology 8: 59
13. Kumagai N, Yu A, Yashiro H (1997) Solid State Ionics 98: 159
14. Kumagai N, Abe M, Kumagai N, Tanno K (1994) Solid State Ionics 70/71: 451
15. Nagelberg AS, Worrell WL (1979) J Solid State Chem 29: 329
16. Levie R (1967) Adv Electrochem Electrochem Eng 6: 329
17. Randles JEB (1947) Disc Faraday Soc 1: 11
18. Ho C, Raistric ID, Huggins RA (1980) J Electrochem Soc 127: 269
19. Joo S, Raistric ID, Huggins RA (1985) Solid State Ionics 17: 313